

Plasma Sci. Technol. **25** (2023) 114004 (11pp) https://doi.org/10.1088/2058-6272/acd83c

Experimental and numerical investigation on the uniformity of nanosecond pulsed dielectric barrier discharge influenced by pulse parameters

Dongxuan ZHANG (张东璇)[1], **Junxian YU** (余俊贤)[2], **Mengyao LI** (李梦遥)[1], **Jie PAN** (潘杰)[3], **Feng LIU** (刘峰)[1,*] **and Zhi FANG** (方志)[1]

[1] College of Electrical Engineering and Control Science, Nanjing Tech University, Nanjing 211816, People's Republic of China
[2] School of Electric Power, South China University of Technology, Guangzhou 510641, People's Republic of China
[3] School of Physics and Electronics, Shandong Normal University, Jinan 250014, People's Republic of China

E-mail: f.liu_1@njtech.edu.cn

Received 3 February 2023, revised 23 May 2023
Accepted for publication 23 May 2023
Published 7 July 2023

Abstract

Nanosecond (ns) pulsed dielectric barrier discharge (DBD) is considered as a promising method to produce controllable large-volume and high activity low-temperature plasma at atmospheric pressure, which makes it suitable for wide applications. In this work, the ns pulse power supply is used to excite Ar DBD and the influences of the pulse parameters (voltage amplitude, pulse width, pulse rise and fall times) on the DBD uniformity are investigated. The gas gap voltage (U_g) and conduct current (I_g) are separated from the measured voltage and current waveforms to analyze the influence of electrical parameters. The spectral line intensity ratio of two Ar excited species is used as an indicator of the electron temperature (T_e). The time resolved discharge processes are recorded by an intensified charge-coupled device camera and a one-dimensional fluid model is employed to simulate the spatial and temporal distributions of electrons, ions, metastable argon atoms and T_e. Combining the experimental and numerical results, the mechanism of the pulse parameters influencing on the discharge uniformity is discussed. It is shown that the space electric field intensity and the space particles' densities are mainly responsible for the variation of discharge uniformity. With the increase of voltage and pulse width, the electric field intensity and the density of space particles increased, which results in the discharge mode transition from non-uniform to uniform, and then non-uniform. Furthermore, the extension of pulse rise and fall times leads to the discharge transition from uniform to non-uniform. The results are helpful to reveal the mechanism of ns pulsed DBD mode transition and to realize controllable and uniform plasma sources at atmospheric pressure.

Keywords: nanosecond pulse, dielectric barrier discharge, electrical characteristics, active particle, uniformity

(Some figures may appear in colour only in the online journal)

* Author to whom any correspondence should be addressed.

1. Introduction

Dielectric barrier discharge (DBD) can generate stable atmospheric non-thermal plasma in large volumes [1, 2], which makes it a wide application prospect in different fields such as material surface modification [3–5], ozone generation [6, 7], pollution control [8–10] and food processing [11, 12]. However, at atmospheric pressure, most DBDs stay in a filamentary mode with lots of short-lived random micro discharge channels in the discharge space [13]. Most of the electric energy and the generated active particles are confined within those filaments, which can cause problems of low energy efficiency, inhomogeneous treatment, and local overheating in practical industrial applications [14]. To enhance the discharge uniformity, researchers usually adopt inert gases (He, Ar, etc) [15], optimize the electrode structure (mesh electrode, water electrode, etc) [16, 17], choose proper dielectric materials (electret material, porous alumina ceramic, etc) [18, 19], and introduce gas flow in the discharge gap to take off heat and impurity [20]. In recent years, with the development of pulsed power technology, the nanosecond (ns) power supply is widely used in plasma excitation and has demonstrated its potential for the generation of a controllable and uniform plasma source [21].

Compared with AC DBD, ns pulsed DBD can improve the discharge uniformity and energy efficiency by its features of overvoltage breakdown, short discharge duration, and long discharge interval [22–25]. In addition, it can effectively overcome the problems of heating damage of the barrier dielectric and the treated materials [24, 26]. The researchers found that adjusting pulse parameters had complex effects on the DBD discharge characteristics. Lu *et al* investigated the effects of the pulse width on the DBD characteristics and discovered that discharge current was significantly affected by pulse widths shorter than 600 ns [27]. Wang *et al* explored the time evolution of ns pulsed DBD and found that using the lower voltage at high frequency or lower frequency at high voltage would be more conducive to achieving stable and uniform discharge [28]. To investigate the impact of voltage and frequency on the particle density of Ar DBD, Pan *et al* developed a one-dimensional fluid model, which showed the density of particles increased with the increase of voltage and frequency [29]. Pourali *et al* used the multispecies fluid model to study the plasma parameters of ns pulsed DBD under different rise and fall times and different pulse widths, and found that with the increase of pulse width and rise time, the electron and ion density increased, while the change of fall time had no significant effect on plasma parameters [30].

The above studies show that the pulse parameters have a significant impact on the discharge process of ns pulsed DBD, which affects discharge uniformity and the reactivity of DBD. Adjusting pulse parameters mainly affects the discharge process by changing the space electric field intensity and the distribution of space particles [31–33]. The applied voltage and the pulse rise time significantly affect the value of breakdown voltage, which determines the space electric field and plasma chemical reaction rate. The pulse width affects the time of the voltage on the electrodes and also the interval time of the two discharges on the rise and fall edges in one pulse period. The pulse fall time affects the development process of second discharge. However, the majority of earlier investigations on ns pulsed DBD focused on the observation of experimental phenomena, the improvement of the application effects, and the realization of uniform discharge at specific experimental conditions. There is a lack of comprehensive studies on the mechanism of the ns pulsed DBD mode transition at different pulse parameters, which prevents the realization and application of uniform and reactive plasmas at atmospheric pressure.

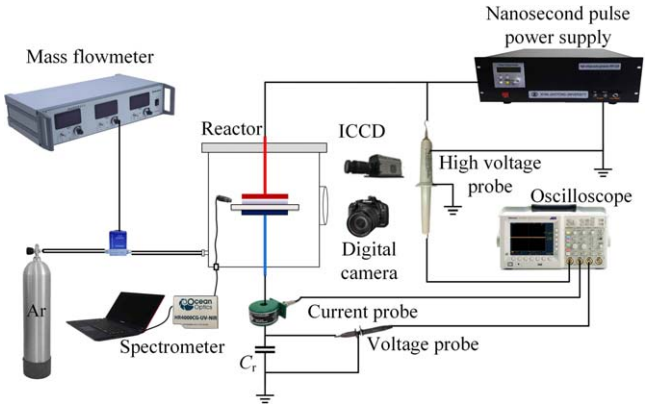

Figure 1. Diagram of experimental device and measurement system.

In this work, the influence of pulse parameters (voltage amplitude, pulse width, and rise and fall times) on the uniformity of ns pulsed DBD is investigated by experimental diagnosis and one-dimensional fluid model simulation. The electrical parameters are obtained through separating the measured voltage and current waveforms. The plasma reactivity and the trend of electron temperature (T_e) are evaluated by the measured optical emission spectra and the ratio of the two specific Ar spectral intensity. The spatial and temporal distributions of electrons, ions, metastable argon atoms and T_e are simulated by the one-dimensional fluid model. With the obtained experimental and simulated results, the mechanism of the pulse parameters influencing on the discharge uniformity of Ar DBD is discussed.

2. Experimental setup and results

2.1. Experimental setup

The experimental setup is shown in figure 1, which has been reported in our previous work [34]. The DBD electrode is placed in the center of the stainless-steel reactor, which can be vacuumed with a rotary pump. The DBD electrode structure includes two circular plate electrodes with a diameter of 50 mm and a quartz glass dielectric with a diameter of 80 mm on the grounded side. The gas gap is fixed at 2 mm. A ns pulse power supply is used to ignite discharge. The output voltage is in the range of 0–15 kV, the pulse width is between 0 and 5000 ns, and the pulse rise and fall times are in the range of 50–500 ns. During experiment, the pulse repetition

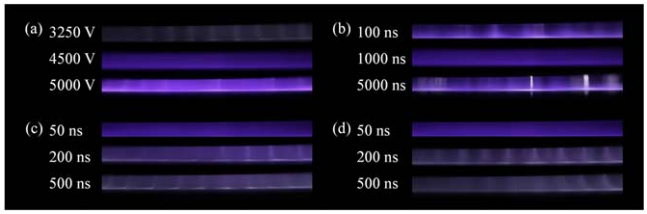

Figure 2. Discharge images of ns pulsed DBD under (a) different voltages at 1000 ns pulse width, 50 ns rise and fall times, (b) different pulse widths at 4500 V, 50 ns rise and fall times, (c) different rise times with 4000 V, 1000 ns pulse width and 50 ns fall time, and (d) different fall times at 4000 V, 1000 ns pulse width and 50 ns rise time.

frequency is fixed at 5 kHz. The applied voltage and current are measured by a North Star high voltage probe (PVM-5) and a Pearson current coil (2877). The voltage across the 2.2 nF measuring capacitor (C_r) is measured by a differential probe (Sapphir, LDP-6002), which is used for electrical parameter calculation. All of the signals are recorded by a Tektronix 3054 oscilloscope. Discharge images with long (1/8 s) and short (50 ns) exposure times are taken by a digital camera (Canon EOS 6D) and an intensified charge-coupled device (ICCD, Andor iStar 334 T), respectively. The optical emission spectra are acquired by an Ocean Optic HR4000CG spectrometer with 50 ms integration time. The working gas is high-purity argon (99.999% purity).

2.2. Experimental results

Figure 2 shows the discharge images of ns pulsed DBD obtained at different pulse parameters (voltage amplitude, pulse width, and rise and fall times), which can determine the uniformity of the discharge easily. It can be seen from figures 2(a) and (b) with different voltage amplitudes and pulse widths that at first, there are dim filaments in the discharge space of both discharge images. With the increase of the voltage amplitude and pulse width, the filaments disappear in the discharge space and the discharges stay in uniform mode. When the voltage amplitude and pulse width further increase, the filaments appear again and become bright. Figures 2(c) and (d) show the discharge images with different pulse rise and fall times, and it can be seen that with short pulse rise and fall times (both 50 ns) the discharges are uniform without filaments observed in space. With the extension of the pulse rise and fall times, the discharge becomes weak and the filaments appear in the space, which decreases the discharge uniformity. In addition, a plasma channel can occur uniformly, dispersedly or randomly at different locations in isolation from each other, forming filamentary discharge modes, including stochastically and self-organized discharge modes [35], which can be observed in figure 2.

It can be seen from figure 2 that the pulse parameters have a great influence on the uniformity of DBD, which involves the effects of the space electric field and reactive particles. To reveal the effect of the space electric field of

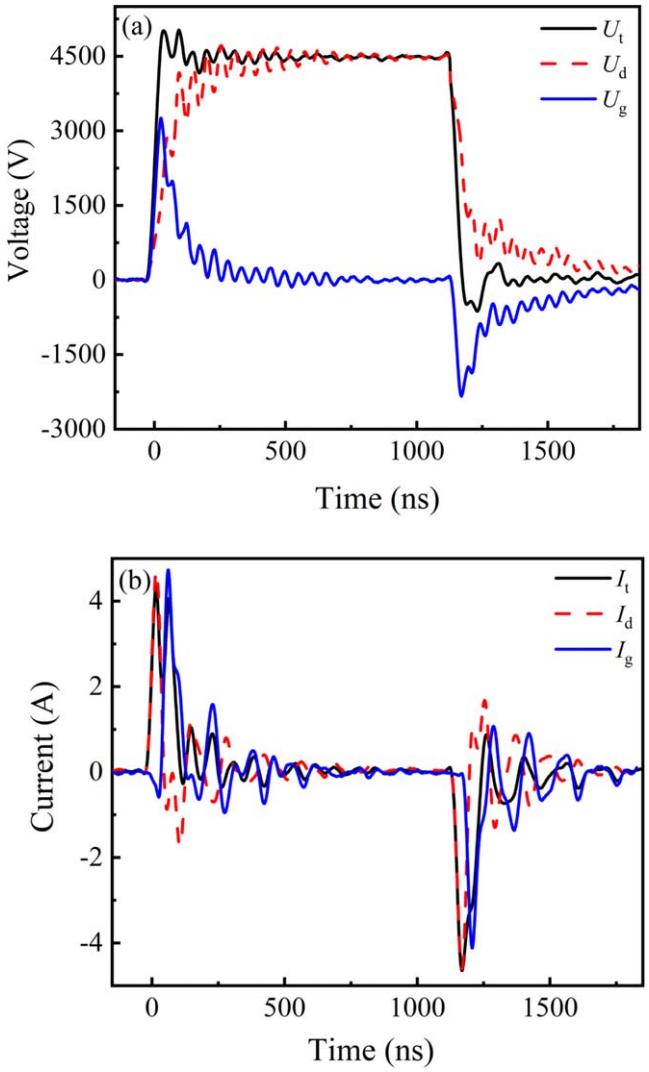

Figure 3. Separation of the voltage (a) and the current (b) waveforms.

DBD, it is necessary to separate the voltage across the gas gap (U_g) from the applied voltage (U_t) for the dielectric barrier acting as a capacitor in the circuit tolerating part of voltage (U_d) from U_t. U_d can be estimated by measuring the voltage across the inserted capacitor C_r (U_m) because both U_d and U_m are the voltages on capacitive loads and there should be an amplification coefficient between them. Considering that the value of U_g will be near zero when the discharge is extinguished, the amplification coefficient can be determined. Then, U_g can be obtained by subtracting U_d from U_t. For the conduction current (I_g), it represents the moving of the space charge and can be obtained by subtracting the displacement current (I_d) from the total current (I_t), I_d can be obtained by extinguishing discharge [36, 37], and the current waveforms are shown in figure 3(b). The waveforms of voltage are shown in figure 3(a).

Figure 3(a) shows the voltage waveforms of U_t, U_g, and U_d and figure 3(b) shows the current waveforms of I_t, I_g, and I_d at 4500 V, 1000 ns pulse width, and 50 ns rise and fall times. It can be seen that at the pulse rise edge of U_t, most of

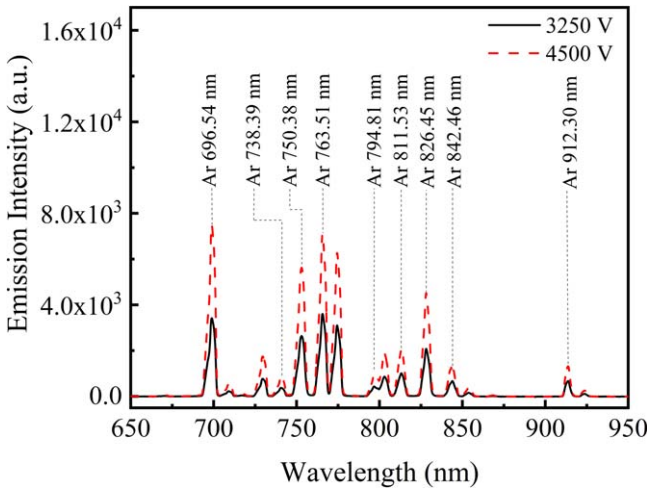

Figure 4. The optical emission spectra of the ns pulsed Ar DBD.

the voltage drops across the gas gap and there is only I_d observed, for the U_g does not reach breakdown value. With the increase of U_g to the breakdown value, the peak of I_g appears and the value of U_g decreases. The duration of the U_g peak is very short at about 100 ns, which can suppress the excessive development of electronic avalanche. With the decrease of U_g to 0, the discharge is distinguished and nearly all of the voltages drop on the dielectric barrier. At the pulse fall edge of U_t, U_d drops slowly for the accumulated charge on the dielectric surface, which leads to a negative U_g peak. When the negative U_g reaches the breakdown value, there is a second discharge with a negative peak of I_g in one pulse.

The optical emission spectrum is recorded to get information on the plasma reactivity. Figure 4 shows the optical emission spectra of the ns pulsed Ar DBD at 3250 V and 4500 V with 1000 ns pulse width, and 50 ns rise and fall times. It can be seen that there are mainly Ar emission lines in the spectra, and the increased voltage enhances the intensity of the Ar lines and makes a change in the ratio of each line, which is related to the electron energy distribution and T_e. The intensity ratio (I_{Ar1}/I_{Ar2}) of two Ar lines (696.54 nm and 912.30 nm)) with different excited energies (13.3 eV and 12.9 eV) is calculated for determining the trend of T_e [37–40]. A high value of I_{Ar1}/I_{Ar2} means high energy electrons taking more proportion and T_e would be high. A low value of I_{Ar1}/I_{Ar2} means low energy electrons taking more proportion and T_e would be low. Therefore, the trend of T_e can be determined from the optical emission spectra observation.

The changes in the space electric field, breakdown characteristics and plasma characteristics caused by the change of pulse parameters result in the change of DBD uniformity. Table 1 shows the two peak values of U_g (U_{g1} and U_{g2}) at the rise and fall edges, and the two peak values of I_g (I_{g1} and I_{g2}) at the experimental conditions of figure 2, which reveals the space electric field intensity at the breakdown moment and the electron density in the gap. The intensity ratios I_{Ar1}/I_{Ar2} at different pulse parameters are also included as an indicator of the variation of T_e.

Table 1 shows that when U_t increases from 3250 to 5000 V, U_{g1} rises from 1674 to 3709 V, and U_{g2} rises from 1199 to 2922 V. It means the reduced electric field (E/n) gradually increases, which results in the increase of T_e as shown in I_{Ar1}/I_{Ar2} increasing from 3.55 to 3.68. This leads to the increase of the electron energy and the reaction rates, thus promoting the development of electron avalanche and enhancing the electron density. Therefore, I_{g1} rises from 1.50 to 5.22 A, and I_{g2} rises from 1.60 to 4.86 A. Low U_t (3250 V) results in weak discharge, so that only weak filamentary discharges can be maintained and the discharge uniformity is poor. Along with the increase of U_t and the enhancement of the spatial electric field strength, the electron density increases, which contributes to the fast expansion and overlapping of the discharge channels, and the plasma diffusing in the gap [41, 42]. The DBD develops from filamentary mode to uniform mode until the plasma fills the entire discharge space. With a further increase of the voltage (5000 V), the spatial electric field intensity is too strong and the charged particles become too much, causing the electron avalanche to develop excessively to form streamer discharge [43], and the high-density charged particles greatly affect the electric field distribution, resulting in electric field distortion, which makes DBD produce a large number of bright filaments. The essential difference between the voltage amplitudes increases from 3250 to 4500 V and that from 4500 to 5000 V should be the development of the electron avalanches.

The pulse width is related to the discharge interval between the first and second discharges in one pulse cycle, thereby affecting the coupling effect between the two discharges. Table 1 shows that while U_{g2} and I_{g2} have a greater increase with increasing the pulse width, the first discharge (U_{g1} and I_{g1}) is less affected. It is because with the extension of the pulse width, the space charges are recombined and the excited reactive species are decayed, which require a higher breakdown voltage in the reverse discharge. Therefore, U_{g2} increases from 1569 to 2513 V with the pulse width increasing from 100 to 5000 ns, which results in the increase of electron density and electron temperature. Then, I_{g2} increases from 2.06 to 4.06 A and I_{Ar1}/I_{Ar2} increases from 3.20 to 3.62. When the pulse width is too short, the discharge intensity of the reverse discharge at the pulse's fall edge is weak, and the electron avalanche is not enough to achieve uniform discharge. With the pulse width increasing, the reverse discharge is further enhanced, both discharges enter the uniform mode, and the plasma looks uniform. When the pulse width is too long, the discharge on the fall edge is strengthened and forms filaments.

The increase in the pulse rise and fall times will cause a change in the pulse voltage rate, affecting the value of the breakdown voltage. When the rise time is extended from 50 to 500 ns, U_{g1} decreases from 2373 to 2096 V, causing the decrease of E/n and T_e, which restricts the electrons from gaining energy and generates fewer free electrons, and I_{g1} decreases significantly from 3.68 to 1.60 A. However, the second discharge is less affected. U_{g2} and I_{g2} are maintained

Table 1. The plasma characteristics of ns pulsed DBD at different pulse parameters.

Pulse parameters		U_{g1} (V)	U_{g2} (V)	I_{g1} (A)	I_{g2} (A)	I_{Ar1}/I_{Ar2}
U_t (kV)	3250	1674	1199	1.50	1.60	3.55
	4500	2828	2028	4.07	3.20	3.55
	5000	3709	2922	5.22	4.86	3.68
Width (ns)	100	2960	1569	3.98	2.06	3.20
	1000	2828	2038	4.06	3.24	3.49
	5000	2708	2513	4.10	4.06	3.62
Rise time (ns)	50	2373	1834	3.68	2.87	3.57
	200	2276	1828	2.40	2.60	3.44
	500	2096	1886	1.60	2.52	3.39
Fall time (ns)	50	2373	1834	3.68	2.87	3.57
	200	2290	1647	3.60	1.80	3.46
	500	2224	1527	3.60	0.69	3.47

at around 1800 V and 2.60 A, respectively. For the decrease of the electron density in the first discharge significantly, it is difficult for the discharge to fill the entire gap at the same time, and dim filaments appear in space. On the contrary, the increase of the pulse fall time has little effect on the first discharge, U_{g1} and I_{g1} are about 2300 V and 3.60 A within 50–500 ns pulse fall time. With the increase of the pulse fall time, the breakdown voltage U_{g2} decreases from 1834 to 1527 V, which decreases E/n in space in the pulse fall edge. Therefore, the peak value of I_{g2} decreases from 2.87 to 0.69 A and I_{Ar1}/I_{Ar2} also decreases. Long pulse fall time makes few accumulated charges on the barrier participating in the second discharge, which lowers the breakdown voltage and electron density. Therefore, the discharge uniformity decreases for the insufficient electrons.

3. Fluid model and numerical simulation

3.1. Discharge processes

From the above experimental results, it can be seen that the parameters affect the discharge uniformity and plasma characteristics by influencing discharge processes at the pulse rise and fall edges. Therefore, the schematic diagram of electric field distribution and charge evolution of the ns pulsed Ar DBD gap in one cycle is given in figure 5 and the discharge process is discussed. Meanwhile, the ICCD images of the discharge processes at the pulse rise and fall edges are shown in figure 6 to support the discussion.

For the pulse rise edge, figure 5(a) shows the moment before the first breakdown discharge occurs in the gap. Under the applied electric field, the gas is ionized, and the ionization coefficient mainly depends on the electric field strength. Figure 5(b) is the moment of the first discharge occurring. The electric field accelerates the electrons to the instantaneous anode, and the electrons continue to collide with argon atoms, resulting in electron avalanches. Figure 5(c) shows the distribution after the first discharge. After the electron avalanche develops to the entire gas gap, the discharge is quickly extinguished because the electric field strength is

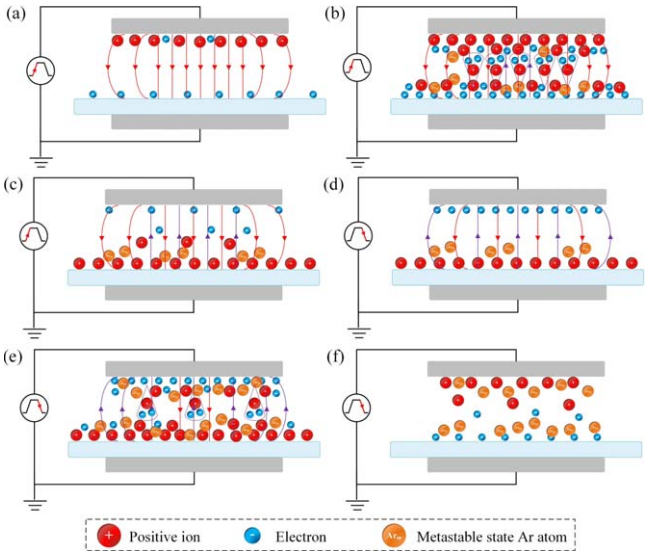

Figure 5. The discharge processes at the pulse rise and fall edges.

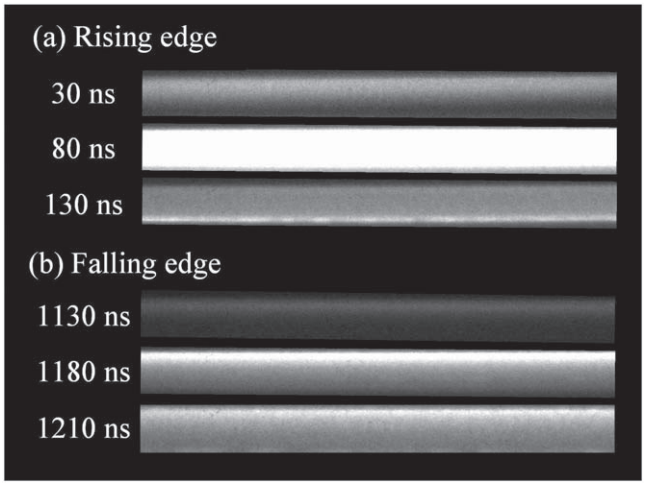

Figure 6. ICCD images of ns pulsed Ar DBD at (a) pulse rise and (b) fall edges at a voltage of 4500 V, pulse width of 1000 ns, and rise and fall time of 50 ns.

reduced to an insufficient level to sustain the discharge. After the current pulse ends, the electric field in the gap tends to be uniformly distributed due to the residual charge. Correspondingly, figure 6(a) shows the ICCD images of the pulse rise edge with 50 ns time resolution. At the beginning of the discharge, the electric field near the anode is high, and a weak light-emitting thin layer is generated near the anode, which then develops into the whole gap. Subsequently, a light-emitting thin layer appears near the cathode as a result of the accumulated charges on the dielectric surface. Eventually, the discharge is extinguished for the decrease of the electric field strength.

For the pulse fall edge, figure 5(d) shows the moment before the second breakdown discharge occurs in the gap. It can be seen that the residual charges and metastable particles on the dielectric surface and space after the first discharge on the pulse rise edge will affect the discharge process on the

pulse fall edge [44]. With the decrease of U_t, the reverse electric field intensity is enhanced until the second breakdown. When the second breakdown occurs, similar as the first discharge, the ionization happens and the electron avalanche develops, as shown in figure 5(e). Figure 5(f) shows that after the second discharge, the residual charge recombines and dissipates. Figure 6(b) also shows the spatiotemporal evolutions of the reverse discharge. Different from the first, the luminescent thin layer appears at the high voltage electrode, because the electrons mainly come from the secondary electron emission from the metal electrode.

From the discussion of the discharge processes and the observed ICCD images, it can be seen that the electric field and the space particles are key factors, which affect the discharge process and uniformity. Because the electric field can be determined by an experimental method, the information of particles needs to be achieved to understand the mechanism of the pulse parameters on discharge uniformity [45, 46]. For the difficulty of experimental diagnosis, a one-dimensional fluid model is employed to simulate the spatial and temporal evolutions of electrons, ions, metastable argon atoms and T_e. Although a one-dimensional model can only simulate uniform distribution and cannot simulate the filamentary mode, the simulated results combined with the experimental results can still give information about the effects of the plasma parameters and pulse parameters on the discharge mode [47, 48].

3.2. Fluid model

Figure 7 shows the geometric diagram of ns pulsed Ar DBD for the simulation similar to the experimental setup. The upper electrode is connected to the output of the pulse power supply, and the lower electrode is connected to the ground with a quartz dielectric barrier cover. d_g represents the discharge gap distance and d_s represents the dielectric thickness.

There are six kinds of particles considered in this model: ground state argon atoms (Ar), electrons (e), 4 s metastable state atoms (Ar_m), argon ions (Ar^+), 4 s resonant state argon atoms ($Ar(^4s)$) and 4p excited state argon atoms ($Ar(^4p)$). The model includes the coupled equations of charge species continuity, the electron energy transmission and the current conservation equation. The space-temporal evolution of various particles is indicated by the following equation.

$$\frac{\partial n_j(x,t)}{\partial t} + \nabla \Gamma_j(x,t) = S_j(x,t) \tag{1}$$

where n is the density, Γ is flux density, S is the source term, j = e, i, ^{4}s, m, ^{4}p (e, i, ^{4}s, m, ^{4}p represent electrons, ions, resonant argon atoms, metastable argon atoms, and excited argon atoms, respectively). The flux density can be obtained from the following momentum equation.

$$\Gamma_j(x,t) = -D_j \nabla n_j(x,t) \pm \mu_j E(x,t) n_j(x,t) \tag{2}$$

where D and μ are the diffusivity and mobility corresponding to the particle, respectively, and μ of neutral particles is 0. E is the electric field intensity, which is determined by the current

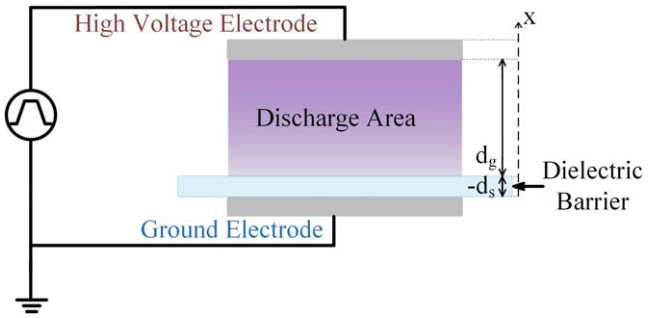

Figure 7. Geometric diagram of ns pulsed Ar DBD.

conservation equation and given as

$$\frac{\partial E(x,t)}{\partial t} = \frac{J_0(t) - J_g(x,t)}{\varepsilon_0} \tag{3}$$

$$J_0 = \frac{\int_0^{d_g} J_g(x,t)\mathrm{d}x - \varepsilon_0 \frac{\partial U_t(t)}{\partial t}}{d_g + \frac{d_s}{\varepsilon_r}} \tag{4}$$

$$J_g = e(\Gamma_i(x,t) - \Gamma_e(x,t)) \tag{5}$$

where J_g is the conduction current density, J_0 is the total current density, and ε_0 is the vacuum dielectric constant.

The electron temperature (T_e) satisfies the electron energy conservation equation, taking the form of

$$\frac{\partial\left(\frac{3}{2}K_B T_e(x,t) N_e(x,t)\right)}{\partial t} + \nabla Q + e\Gamma_e(x,t) E_e(x,t) + e\sum_i \Delta\varepsilon_i(x,t) r_i(x,t) = 0 \tag{6}$$

$$Q = -\frac{5}{2}K_B D_e N_e(x,t)\nabla T_e(x,t) + \frac{5}{2}K_B T_e(x,t)\Gamma_e(x,t) \tag{7}$$

where K_B is the Boltzmann constant, $\Delta\varepsilon_i$ and r_i denote the energy loss and reaction rate of the ith reaction, respectively. Table 2 shows the important reactions and the corresponding reaction rates in the ns pulsed Ar DBD.

Considering the secondary electron emission from the dielectric and the electrode surface, the electron flux density at this position needs to be updated by

$$\Gamma_e'(x,t) = \Gamma_e(x,t) - \gamma\sum_i \Gamma_i(x,t) \tag{8}$$

where γ is the secondary electron emission coefficient. The fluid model is a self-programmed FORTRAN code. More details of the fluid model and initial conditions can be found in [51–55]. The limitation of the fluid model is that it cannot accurately capture the kinetic effects of pulsed discharge with the pulse rising phase less than 100 ns. But the simulation results can still help explain the experimental phenomena.

3.3. Spatial and temporal distributions of particles

The voltage and current waveforms obtained through the simulation model under the same experimental conditions of figure 3 (4500 V, 1000 ns pulse width, and 50 ns rise and fall times) are shown in figure 8. I_d is calculated by U_d from the

Table 2. The important reactions in the ns pulsed Ar DBD.

No.	Reaction equation	Reaction rate coefficient	References
1	$Ar + e \rightarrow Ar_m + e$	$2.5 \times 10^{-9} T_e^{0.74} \exp(-11.56/T_e)$ cm^3 s^{-1}	[49]
2	$Ar + e \rightarrow Ar^+ + 2e$	$2.3 \times 10^{-8} T_e^{0.68} \exp(-15.76/T_e)$ cm^3 s^{-1}	[49]
3	$Ar + e \rightarrow Ar(^4s) + e$	$2.5 \times 10^{-9} T_e^{0.74} \exp(-11.56/T_e)$ cm^3 s^{-1}	[49]
4	$Ar + e \rightarrow Ar(^4p) + e$	$1.4 \times 10^{-8} T_e^{0.71} \exp(-13.2/T_e)$ cm^3 s^{-1}	[49]
5	$Ar_m + e \rightarrow Ar^+ + 2e$	$6.8 \times 10^{-9} T_e^{0.67} \exp(-4.2/T_e)$ cm^3 s^{-1}	[49]
6	$Ar_m + e \rightarrow Ar + e$	$4.3 \times 10^{-10} T_e^{0.74}$ cm^3 s^{-1}	[49]
7	$Ar_m + e \rightarrow Ar(^4s) + e$	2×10^{-7} cm^3 s^{-1}	[49]
8	$Ar_m + e \rightarrow Ar(^4p) + e$	$8.9 \times 10^{-7} T_e^{0.51} \exp(-1.59/T_e)$ cm^3 s^{-1}	[49]
9	$Ar(^4s) + e \rightarrow Ar^+ + 2e$	$6.8 \times 10^{-9} T_e^{0.67} \exp(-4.2/T_e)$ cm^3 s^{-1}	[49]
10	$Ar(^4s) + e \rightarrow Ar + e$	$4.3 \times 10^{-10} T_e^{0.74}$ cm^3 s^{-1}	[49]
11	$Ar(^4s) + e \rightarrow Ar_m + e$	3×10^{-7} cm^3 s^{-1}	[49]
12	$Ar(^4s) + e \rightarrow Ar(^4p) + e$	$8.9 \times 10^{-7} T_e^{0.51} \exp(-1.59/T_e)$ cm^3 s^{-1}	[49]
13	$Ar(^4p) + e \rightarrow Ar^+ + 2e$	$1.8 \times 10^{-7} T_e^{0.61} \exp(-2.61/T_e)$ cm^3 s^{-1}	[49]
14	$Ar(^4p) + e \rightarrow Ar(^4s)_m + e$	$1.5 \times 10^{-7} T_e^{0.51}$ cm^3 s^{-1}	[49]
15	$Ar(^4p) + e \rightarrow Ar + e$	$3.9 \times 10^{-10} T_e^{0.71}$ cm^3 s^{-1}	[49]
16	$Ar(^4s) \rightarrow Ar + h\nu$	2×10^6 s^{-1}	[49]
17	$Ar_m \rightarrow Ar + h\nu$	2×10^6 s^{-1}	[50]
18	$Ar(^4p) \rightarrow Ar(^4s)_m + h\nu$	3×10^7 s^{-1}	[50]

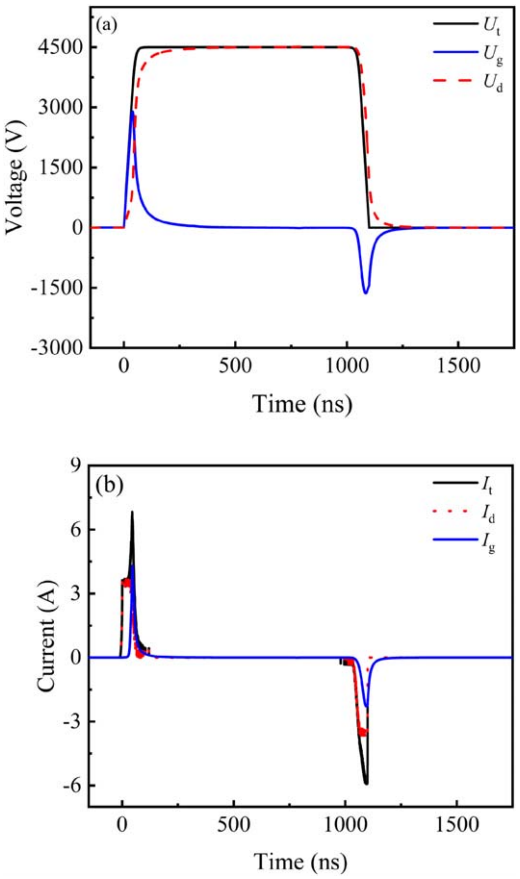

Figure 8. Simulation results of the separation of the voltage and current waveforms.

simulation and the capacitance value of the dielectric barrier is calculated by experimental results. I_g is obtained by equations (4) and (5). Compared with figure 3, the values of U_g and I_g obtained from the simulation model are in good agreement with those obtained from the experiment. It is noticed that there are small ripples in experimental U_g and I_g, and they are produced by the nonstandard output voltage waveform, which results from the stray capacitance and inductance in the internal circuit of the power supply. In simulation, we adopt a standard pulse voltage waveform to perform simulation. Therefore, there is no ripple in simulated U_g and I_g. The discharge process mainly depends on the peak values of U_g and I_g. Therefore, the missing ripple has no significant effect on the electrical parameters, which can be used to simulate the evolution of particles.

The spatial and temporal distributions of the electron density (n_e), ion density (n_i), T_e, and Ar_m density (n_m) at the experimental conditions of 4500 V, 1000 ns pulse width, and 50 ns rise and fall times are shown in figure 9. It can be seen that the n_e, n_i, T_e, and n_m show two peaks during the pulse voltage corresponding to the two discharges at the pulse rise and fall edges. After the breakdown of the gas gap, the n_e increases rapidly. Initially, with the help of the external electric field, a large number of electrons move to the momentary anode, causing a significant space charge effect. Subsequently, it leads to the faster movement of high-energy electrons in the gas gap to the momentary cathode, forming a cathode sheath, which accelerates the decline of the U_g and the extinction of the discharge. Furthermore, the temporal and spatial distribution trend of ion and T_e is consistent with that of electrons, but the peak value of n_i is larger than that of n_e.

During the first discharge, the n_e increases rapidly, and the electrons collide with the argon atoms to generate Ar_m. After that, the discharge is extinguished, and n_e decreases rapidly. However, Ar_m has a longer life time and decays much more slowly, and n_m remains almost unchanged. Until the reverse discharge occurs, the n_e increases again and promotes the occurrence of related plasma reactions, resulting in the further increase of the n_m and maintaining the time on the millisecond scale. In addition, the peak of the n_m is much

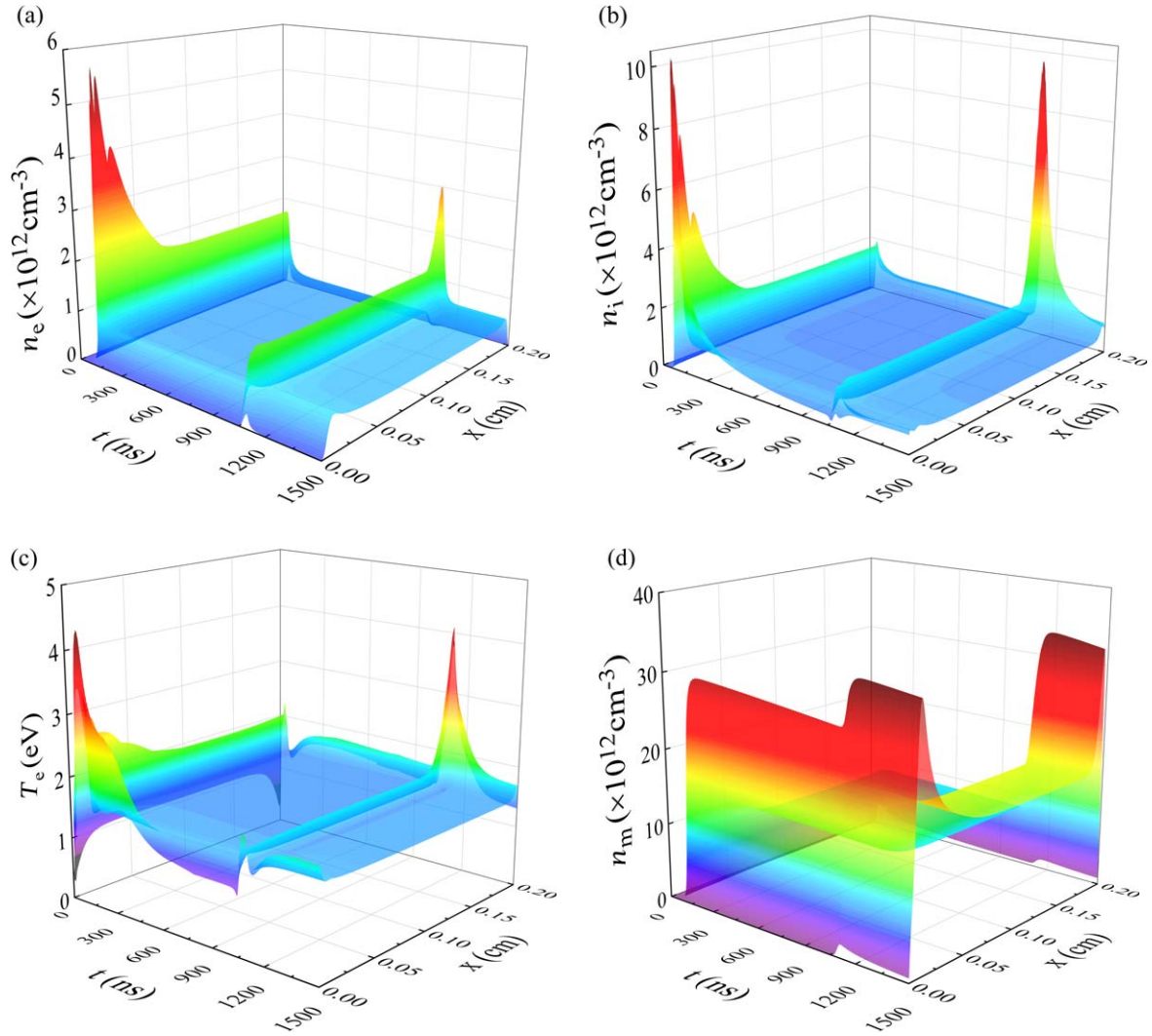

Figure 9. Spatiotemporal evolutions of (a) electronics density distributions, (b) ions density distributions, (c) T_e distributions, and (d) Ar_m density distributions.

higher than the peak of the n_e, and the electrically neutral Ar_m will not be subject to drift induced by the electric field, which has a more uniform distribution in the discharge region. Therefore, the Ar_m in the gap has a profound influence on the generation and development of the discharge and uniformity.

3.4. Effect of pulse parameters on particles densities

In section 3.3, the spatial and temporal distributions of n_e, n_i, T_e, and n_m have been simulated in specific experimental conditions. In order to understand the influences of the pulse parameters on the discharge processes and uniformity, n_{e1}, n_{e2}, n_{i1}, n_{i2}, T_{e1}, T_{e2}, n_{m1} and n_{m2} are simulated at different voltage amplitudes, pulse widths, and rise and fall times as shown in figure 10, in which the n_{e1}, n_{i1}, T_{e1}, n_{m1} and n_{e2}, n_{i2}, T_{e2}, n_{m2} represent the maximum values of n_e, n_i, T_e and n_m at the pulse rise and fall edges, respectively.

The simulated results in figure 10 are consistent with the experimental results, and the increase of voltage amplitude has a significant improvement in the space particle density. As the voltage increases, the total current density increases, the space electric field strength increases, and the value of E/n increases. As the T_e rises, the electrons gain more energy, which leads to the increase of collision frequency between electrons and particles, and improves the efficiency of generating active particles. Compared with the first discharge, the increase of n_{e2} and n_{i2} is relatively small. This may be caused by the impact of residual charge after the first discharge. However, for the long lifetime of Ar_m, both of the two discharges are beneficial to enhance n_m. Therefore, the n_{m2} is much too high. When the voltage amplitude is low, n_e and n_m are less, and the distribution is inhomogeneous. The electron avalanches cannot fill the whole discharge space at the same time. When the voltage amplitude is high, the n_e is too high and the spatial electric field distortion is serious, which is very easy to form streamer discharge and reduce the discharge uniformity.

The increase of pulse width mainly affects the discharge process at the pulse fall edge, which leads to the increase of n_{e2} and T_{e2}, n_{i2} increasing first and then decreasing, and the decrease of n_{m2}. With the increase of the pulse width,

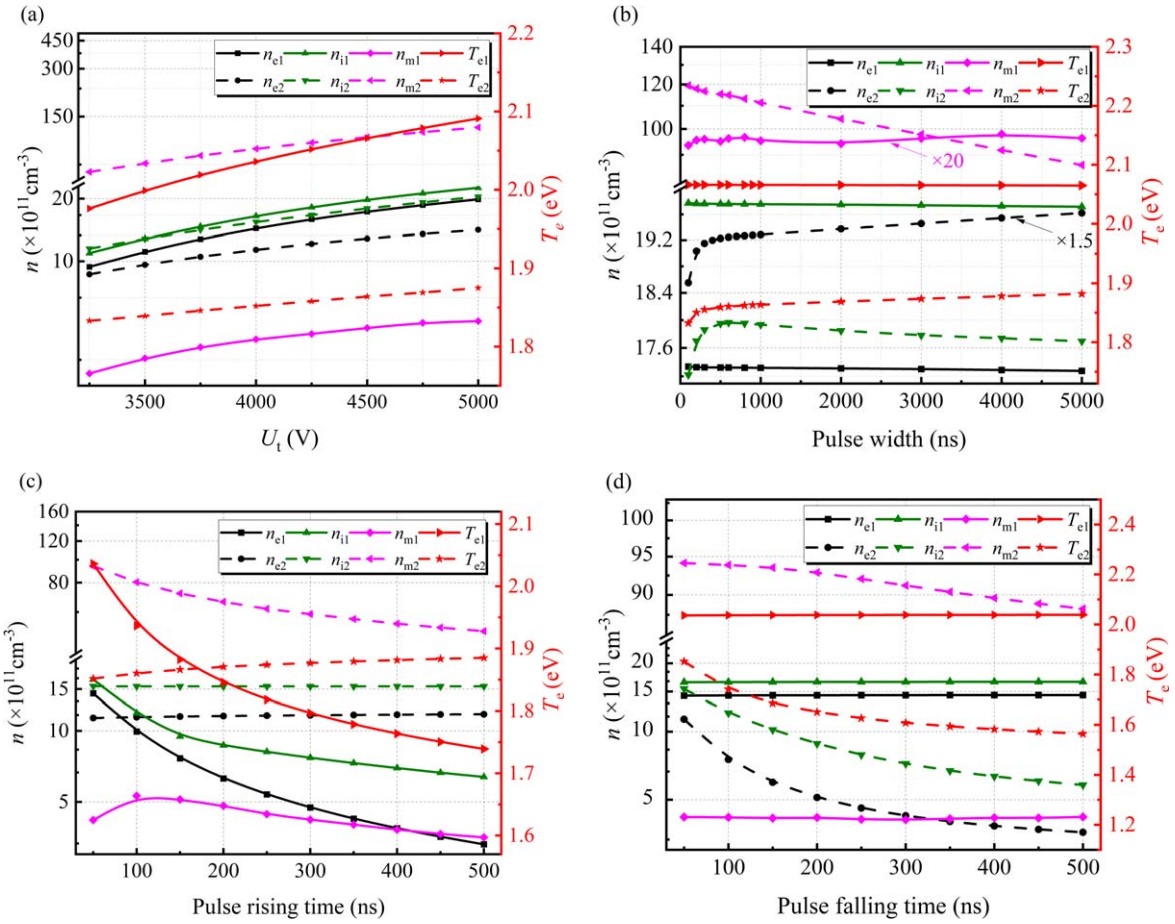

Figure 10. n_{e1}, n_{e2}, n_{i1}, n_{i2}, T_{e1}, T_{e2}, n_{m1}, n_{m2} at different (a) voltage amplitudes, (b) pulse widths, (c) rise times, and (d) fall times.

the interval time between the finish of the first discharge and the occurrence of the second discharge becomes longer, n_e, n_i, and n_m decrease before the second discharge for the quenching with background gas, which results in the increase of the breakdown voltage at the pulse fall edge. With a high breakdown voltage, n_{e2}, n_{i2}, and T_{e2} increase. But the increase of the pulse width also causes more time dissipation and recombination of electrons and ions. In addition, the reduction of Ar_m causes the weakening of multi-step ionization. When the pulse width is increased to more than 600 ns, the n_i slightly decreases, and the n_e and T_e rise rates become smaller. When the pulse width is short, n_{e2} is small, and the electron avalanches are insufficient to cover the whole space. The discharge image shows non-uniform with dim stripes. When the pulse width is too long, the space lacks Ar_m, which increases the breakdown voltage. Therefore, under a high electric field, bright filaments are formed, which decreases the discharge uniformity.

The adjusting of the pulse rise time would change the breakdown voltage value, and then affect n_e, n_i, T_e, and n_m. From figure 10(c), it can be seen that with the increase of the pulse rise time, n_{e1} and n_{i1} decrease, n_{m1} first increases and then decreases, n_{e2} increases slightly, and n_{m2} decreases. It is because with the increase of the pulse rise time, the breakdown voltage decreases, resulting in the decrease of E/n and T_{e1}, the excitation and ionization processes are weakened, and fewer electrons and ions are generated. Because the discharge time increases with the increasing rise time, the competition between the generation of Ar_m by electrons and argon atom collision and the quenching of Ar_m by the argon atom causes the n_{m1} to first increase and then decrease. Due to the effect of Ar_m multi-step ionization, n_{e2} increases slightly, and n_{m2} decreases. Finally, due to the low electron density of the first discharge at the pulse rise edge, the discharge is insufficient with space with dim stripes in space. The change of the pulse fall time only affects the second discharge at pulse fall edge. As seen from figure 10(d), n_{e1}, n_{i1}, n_{m1} and T_{e1} are almost unchanged. With the increase of pulse fall time, the breakdown voltage decreases, which decreases E/n and then results in the decline of n_{e2}, n_{i2}, n_{m2} and T_{e2}. Therefore, a long pulse fall time leads to poor discharge uniformity.

The previous works mostly focused on the determination of the experimental parameters [56, 57] and electrode configurations [58, 59] for the realization of the uniform mode of ns pulsed DBDs and they attributed the mechanisms to the properties of pulsed discharge, such as a high E/n to promote electron avalanche [60] and short discharge duration to prevent streamer development [43, 61]. Our research is also based on the optimized experimental parameters for the realization of the uniform discharge mode, but further explores the influences of experimental parameters on the discharge process with the

experimental and simulated results. With the help of ICCD observation and numerical simulation of the spatiotemporal evolution of plasma parameters, the evolutions of the spatial electric field and space particles are used to explain the mode transition, which are helpful to further understand the discharge behavior and realize uniform, stable, and reactive plasmas at atmospheric pressure.

4. Conclusion

In this work, the effects of pulse parameters (voltage aptitude, pulse width, rise and fall time) on the uniformity of the ns pulsed Ar DBD are investigated by experimental diagnosis and numerical simulation. It is found that with the increase of voltage aptitude and pulse width, the discharge mode of DBD transitions from non-uniform to uniform, and with a further increase of voltage aptitude and pulse width, the uniform DBD becomes non-uniform again. The increases in pulse rise and fall times would decrease the discharge uniformity. With the separation of voltage and current waveforms and the observation of the optical emission spectra of the ns pulsed Ar DBD, it is found that with the increase of the voltage aptitude, the breakdown voltages at the pulse rise and fall edges increase, which leads to the increase of the current peak value and T_e. Therefore, the discharge becomes uniform from insufficient discharge and then non-uniform with bright filaments. The increase of pulse width would result in the increase of the current peak value at the fall edge for the higher breakdown voltage and T_e. Then, the discharge uniformity becomes better and gets worse with the increase in pulse width. The increases in pulse rise and fall times decrease the breakdown voltages at the pulse rise and fall edges, which decreases the current peak value, T_e, and also the discharge uniformity. With a one-dimensional fluid model, the spatial and temporal distributions and the influences of the pulse parameters of n_e, n_i, T_e and n_m are simulated. The spatial and temporal distributions of the particles are consistent with the observation of an ICCD camera for the discharge processes at the pulse rise and fall edges. The breakdown voltage and the tendencies of n_e, n_i, T_e and n_m vary with the pulse parameters, the space electric field intensity and the space particles' densities are responsible for the variation of discharge uniformity. Less space particles would result in weak discharge with dim strips and more space particles would lead to bright filaments and decrease the discharge uniformity. The results would contribute to the improvement of atmospheric pressure plasma reactivity and discharge uniformity.

Acknowledgments

This work is supported by National Natural Science Foundation of China (Nos. 52177148, 51777091 and 52037004) and Postgraduate Research & Practice Innovation Program of Jiangsu Province (KYCX23_1449).

References

[1] Kogelschatz U 2003 *Plasma Chem. Plasma Process.* **23** 1
[2] Li H *et al* 2021 *Phys. Plasmas* **28** 113505
[3] Dorai R and Kushner M J 2003 *J. Phys. D: Appl. Phys.* **36** 666
[4] Chen W M *et al* 2018 *Prog. Org. Coat.* **125** 128
[5] Ojah N *et al* 2019 *Appl. Surf. Sci.* **475** 219
[6] Li M *et al* 2018 *Vacuum* **157** 249
[7] Homola T *et al* 2019 *Plasma Chem. Plasma Process.* **39** 1227
[8] Tu X and Whitehead J C 2012 *Appl. Catal. B: Environ.* **125** 439
[9] Zhang S *et al* 2022 *High Voltage* **7** 718
[10] Cui Z L *et al* 2022 *High Voltage* **7** 1048
[11] Liu K *et al* 2023 *Plasma Process. Polym.* **20** e2200134
[12] Misra N N and Martynenko A 2021 *Innovative Food Sci. Emerging Technol.* **70** 102672
[13] Liu Y F *et al* 2014 *Appl. Surf. Sci.* **313** 53
[14] Milaniak N, Laroche G and Massines F 2021 *Plasma Processes Polym.* **18** 2000248
[15] Schmitz G J *et al* 2016 *Sci. Technol. Adv. Mater.* **17** 410
[16] Shao T *et al* 2013 *IEEE Trans. Plasma Sci.* **41** 3069
[17] Liu S *et al* 2022 *Curr. Appl Phys.* **44** 12
[18] Osawa N and Yoshioka Y 2012 *IEEE Trans. Plasma Sci.* **40** 2
[19] Liu W Z *et al* 2018 *Plasma Sci. Technol.* **20** 035401
[20] Zeniou A *et al* 2017 *J. Phys. D: Appl. Phys.* **50** 135204
[21] Shao T *et al* 2018 *High Voltage* **3** 14
[22] Yang D Z *et al* 2012 *Plasma Sources Sci. Technol.* **21** 035004
[23] Zhang C *et al* 2013 *IEEE Trans. Dielectr. Electr. Insul.* **20** 1304
[24] Jin S H *et al* 2022 *High Voltage* **7** 98
[25] Jiang H *et al* 2011 *IEEE Trans. Plasma Sci.* **39** 2076
[26] Wang Q *et al* 2018 *Plasma Sci. Technol.* **20** 035404
[27] Lu X P *et al* 2009 *IEEE Trans. Plasma Sci.* **37** 647
[28] Wang Y Y *et al* 2021 *Plasma Sources Sci. Technol.* **30** 075009
[29] Pan J *et al* 2016 *Plasma Sci. Technol.* **18** 1081
[30] Pourali N *et al* 2021 *Phys. Plasmas* **28** 013502
[31] Ayan H *et al* 2009 *J. Phys. D: Appl. Phys.* **42** 125202
[32] Starikovskaia S M *et al* 2001 *Plasma Sources Sci. Technol.* **10** 344
[33] Yang D Z *et al* 2013 *Appl. Phys. Lett.* **102** 194102
[34] Liu F *et al* 2022 *Plasma Sci. Technol.* **24** 054004
[35] Engelhardt M *et al* 2017 *Plasma Process. Polym.* **14** 1600095
[36] Liu F *et al* 2021 *J. Appl. Phys.* **129** 033302
[37] Liu F *et al* 2010 *Plasma Sources Sci. Technol.* **19** 045017
[38] Roy N C *et al* 2021 *Plasma Process. Polym.* **18** 2000087
[39] Calzá M *et al* 2020 *Eur. Phys. J. Plus* **135** 1
[40] Zhu X M and Pu Y K 2010 *J. Phys. D: Appl. Phys.* **43** 403001
[41] Liu C, Dobrynin D and Fridman A 2014 *J. Phys. D: Appl. Phys.* **47** 252003
[42] Babaeva N Y and Kushner M J 2014 *Plasma Sources Sci. Technol.* **23** 065047
[43] Liu C, Fridman A and Dobrynin D 2019 *J. Phys. D: Appl. Phys.* **52** 105205
[44] Callegari T, Bernecker B and Boeuf J P 2014 *Plasma Sources Sci. Technol.* **23** 054003
[45] Liu K *et al* 2022 *Phys. Chem. Chem. Phys.* **24** 8940
[46] Liu K *et al* 2022 *Vacuum* **198** 110901
[47] Golubovskii Y B *et al* 2003 *J. Phys. D: Appl. Phys.* **36** 39
[48] Martens T, Bogaerts A and van Dijk J 2010 *Appl. Phys. Lett.* **96** 131503
[49] Lee M H and Chung C W 2005 *Phys. Plasmas* **12** 073501
[50] Bogaerts A and Gijbels R 1995 *Phys. Rev.* A **52** 3743
[51] Pan J *et al* 2014 *Plasma Sources Sci. Technol.* **23** 065019
[52] Liu F C, He Y F and Wang X F 2014 *Chin. Phys.* B **23** 075209
[53] Qi Y *et al* 2019 *IEEE Trans. Plasma Sci.* **47** 1553
[54] Kulikovsky A A 1994 *J. Phys. D: Appl. Phys.* **27** 2556

[55] Zhang Y T, Liu Y and Liu B 2017 *Plasma Sci. Technol.* **19** 085402
[56] Qi H C *et al* 2016 *Plasma Sci. Technol.* **18** 520
[57] Zhang S *et al* 2014 *Spectrochim. Acta Part A: Mol. Biomol. Spectrosc.* **117** 535
[58] Guo H F *et al* 2018 *Phys. Plasmas* **25** 093505
[59] Gu J W *et al* 2016 *Plasma Sci. Technol.* **18** 230
[60] Yu S *et al* 2016 *Phys. Plasmas* **23** 023510
[61] Zhang S *et al* 2019 *Spectrochim. Acta Part A: Mol. Biomol. Spectrosc.* **207** 294